

Landslides (2020) 17:2795–2809
 DOI 10.1007/s10346-020-01445-z
 Received: 25 June 2019
 Accepted: 28 May 2020
 Published online: 30 June 2020
 © The Author(s) 2020

Erin K. Bessette-Kirton · Jeffrey A. Coe · William H. Schulz · Corina Cerovski-Darriau · Mason M. Einbund

Mobility characteristics of debris slides and flows triggered by Hurricane Maria in Puerto Rico

Abstract Mobility is an important element of landslide hazard and risk assessments yet has been seldom studied for shallow landslides and debris flows in tropical environments. In September 2017, Hurricane Maria triggered > 70,000 landslides across Puerto Rico. Using aerial imagery and a lidar digital elevation model (DEM), we mapped and characterized the mobility of debris slides and flows in four different geologic materials: (1) mudstone, siltstone, and sandstone; (2) submarine basalt and chert; (3) marine volcanoclastics; and (4) granodiorite. We used the ratio of landslide-fall height (H) to travel length (L), H/L, to assess the mobility of landslides in each material. Additionally, we differentiated between landslides with single and multiple source areas and landslides that either did or did not enter drainages. Overall, extreme rainfall contributed to the mobility of landslides during Hurricane Maria, and our results showed that the mobility of debris slides and flows in Puerto Rico increased linearly as a function of the number of source areas that coalesced. Additionally, landslides that entered drainages were more mobile than those that did not. We found that landslides in soils developed on marine volcanoclastics were the most mobile and landslides in soils on submarine basalt and chert were the least mobile. While landslides were generally small (< 100 m²) and displayed a wide range of H/L values (0.1–2), coalescence increased the mobility of landslides that transitioned to debris flows. The high but variable mobility of landslides that occurred during Hurricane Maria and the associated hazards highlight the importance of characterizing and understanding the factors influencing landslide mobility in Puerto Rico and other tropical environments.

Keywords Landslides · Debris flows · Landslide mobility · Travel distance · H/L · Puerto Rico · Hurricane Maria

Introduction

Landslide hazards are largely controlled by the size and location of initiation and the total distance traveled (mobility) after initiation. Landslide mobility is often evaluated by the ratio of landslide-fall height (H) to travel length (L), H/L (e.g., Heim 1932; Corominas 1996), where low values of H/L indicate high mobility and high H/L values indicate low mobility. High mobility landslides that travel long distances are often more hazardous and can pose a greater risk to people or infrastructure downslope (e.g., Corominas 1996; Evans et al. 2007; Iverson et al. 2015; Coe et al. 2016; Kean et al. 2019). Landslide mobility can be controlled by intrinsic factors such as material and pore-pressure characteristics (e.g., Terzaghi 1950; Sassa 1985; Iverson 1997; Davies et al. 1999; Iverson et al. 2015; Manzanal et al. 2016) or source area volume (e.g., Heim 1932; Corominas 1996; Legros 2002). Extrinsic factors such as volume growth through the coalescence of multiple landslides (e.g., Coe et al. 2011b) or material entrainment (e.g., Sassa 1985; Santi and Mathewson 1988; Jibson 1989; Hungr and Evans 2004; Evans et al. 2007; Reid et al. 2016; Collins and Reid 2019) and topographic confinement

and geotechnical characteristics of the landslide travel path (e.g., Legros 2002; Sassa and Wang 2005; Schneider et al. 2011; Aaron and McDougall 2019; Strom et al. 2019) also affect landslide mobility. Rainfall and flooding during prolonged storm events such as hurricanes can also enhance mobility by increasing the water content of landslides.

In tropical environments, including Puerto Rico, previous landslide research has focused on understanding and forecasting landslide initiation (e.g., Monroe 1979; Jibson 1989; Guariguata and Larsen 1990; Larsen and Torres-Sánchez 1992; Collison and Anderson 1996; Larsen and Parks 1998; Larsen and Torres-Sánchez 1998; Harp et al. 2004; Larsen et al. 2004; Liao et al. 2010; Vieira et al. 2010; Lepore et al. 2012), but relatively little effort has focused on understanding and forecasting landslide mobility. A handful of studies have assessed landslide mobility in settings that are similar to Puerto Rico (e.g., Ellen et al. 1993; Dai and Lee 2002; Evans et al. 2007; Devoli et al. 2009), and valuable descriptions of travel distance and runout characteristics from localized landslides in Puerto Rico are provided by Jibson (1989), Jibson (1992), and Larsen and Torres-Sánchez (1992).

In September 2017, Hurricane Maria triggered over 70,000 slope failures, including landslides, slumps, debris flows, and rock falls (Hughes et al. 2019). The majority of failures were shallow (< 5 m) debris slides (e.g., Hungr et al. 2014), many of which mobilized as debris flows that traveled as far as 1.5 km, causing damage to homes, roads, and other infrastructure located downslope and resulting in at least three fatalities (Hennessy-Fiske 2017; Irizarry Álvarez 2017). The threat posed by landslides that travel long distances from where they originate highlights the need for assessments of landslide mobility in tropical mountainous environments during hurricanes as a means of informing hazard forecasting. The widespread occurrence of landslides during this event allowed for an evaluation of landslide mobility across varying terranes, geologic formations, and regolith materials.

To improve the understanding of landslide mobility in tropical environments, we studied debris slides and debris flows in four geologically distinct areas of Puerto Rico following Hurricane Maria (Fig. 1). Except where specified, we simply use the term “landslide” to describe both failure types. For each study area, we mapped headscarp points, affected areas, and travel distances and determined the number of individual source areas contributing to coalescing landslides. This mapping methodology allowed us to characterize landslide mobility with respect to geology, landslide coalescence, and drainage network characteristics. We assessed the influence of coalescence and drainage network interactions on landslide mobility by examining the travel distance characteristics of landslides with single and multiple source areas and landslides that either did or did not enter the drainage network. We used our results to hypothesize about the physical controls potentially responsible for observed variations in mobility and to highlight factors that are important to consider in regional debris-flow inundation assessments.

Hurricane Maria

Hurricane Maria made landfall along the southeast coast of Puerto Rico as a category 4 hurricane with sustained winds of 249 km/h on 20 September 2017 (Pasch et al. 2019). The storm moved across Puerto Rico with a west-northwest trajectory (Fig. 1) and deluged the island with extreme precipitation, causing widespread flooding and landslides. The difficulties associated with collecting accurate rainfall measurements during hurricanes due to strong winds and the inability to measure wind-driven rainfall were compounded during Hurricane Maria by damage to rain gauges (at least 14 of the US Geological Survey's 24 gauge stations; US Geological Survey 2017) and the failure of two Federal Aviation Administration Doppler radars (Buchanan 2017; National Weather Service, 2017). Therefore, rainfall estimates for Hurricane Maria vary both in distribution and magnitude, with maximum values ranging from 733 (Ramos-Scharrón and Arima 2019) to 1029 mm (Keellings and Hernández Ayala 2019). Nonetheless, Hurricane Maria produced the highest total rainfall of any storm to hit Puerto Rico since 1956 (Keellings and Hernández Ayala 2019) and had the largest 24-h rainfall intensity of all recorded storms to affect the island (Ramos-Scharrón and Arima 2019). In addition to the intensity and total amount of rainfall, above-average antecedent soil moisture throughout much of Puerto Rico's mountainous terrain likely contributed to the prevalence of landslides during Hurricane Maria (Bessette-Kirton et al. 2019a).

Study areas

To examine the detailed characteristics of landslides, we mapped landslides in four 2.5-km² study areas where the density of landslides triggered by Hurricane Maria exceeded 25 landslides/km² (Bessette-Kirton et al. 2017, 2019a). The study areas transect the island from east to west and encompass three distinct geologic terranes (Fig. 1; Bawiec 1998). Each study area contains one or more unique geologic formations (Table 1; Krushensky and Schellekens 1998) and includes at least one major road, several minor roads, a major stream, and several watersheds.

The Las Marías 1 (LAM1) study area lies on the boundary of the Mayagüez, Añasco, and Las Marías municipalities (Fig. 1) and is located 9 km northeast of the City of Mayagüez and 8 km west of the town of Las Marías. LAM1 is underlain by marine volcanoclastic terrane, and nearly all landslides occurred in soil and saprolite developed on the Yauco Formation (TKy; Table 1, Fig. 2). The Las Marías 2 (LAM2) study area is bisected by the municipalities of Las Marías and Lares (Fig. 1) and is located 7 km east of the town of Las Marías and 6 km southwest of the town of Lares. LAM2 is underlain by submarine basalt and chert terrane, and bedrock geology consists of the Concepcion Formation (Kco; Table 1, Fig. 2). The Utuado (UTU) study area is located 1 km north of the town of Utuado and is underlain by intrusive terrane (Table 1). Bedrock geology consists of granodiorite of the Utuado batholith (Ku; Table 1, Fig. 2). The Naranjito (NAR) study area is located 2 km west of the town of Naranjito and is underlain by marine volcanoclastic terrane (Table 1). The predominant bedrock geologic unit in NAR is the Los Negros Formation (Kln; Table 1, Fig. 2).

Methods

Landslide mapping

Using ~0.15-m resolution natural color aerial imagery collected by the Federal Emergency Management Agency (FEMA) from 9 to 15 October 2017 (Quantum Spatial, Inc. 2017), we mapped landslide polygons, headscarp points at the top of landslide source areas,

and travel distance lines, at scales between 1:600 and 1:1000 (Bessette-Kirton et al. 2019b). Landslides were readily identifiable in aerial imagery because of the widespread defoliation caused by Hurricane Maria and the stark color contrast between soil or rock and vegetation. We mapped landslides by identifying areas of exposed soil or rock with geomorphic characteristics typical of landslides (e.g., arcuate scarps and flow paths).

Landslide polygons were drawn by delineating the total area disturbed by a landslide (including source, travel path, and deposit area). For each landslide polygon, we mapped at least one headscarp point (Fig. 3a) by identifying the center of the landslide headscarp. Many landslide polygons included multiple connected (Fig. 3b) and/or coalescing (Fig. 3c) landslides. In such cases, we mapped headscarp points for each identifiable landslide headscarp. Although multiple headscarp points (up to 55 in the UTU study area) were contained within a single landslide polygon, we could not determine the temporal sequence of landslides or whether individual failures occurred simultaneously or were separated in time. We field checked ~30% of landslides in each study area (including source areas and runout paths) to evaluate the types of landslides (debris slides and flows) and to confirm our remote mapping.

The aerial imagery that we used to map landslide polygons was rapidly acquired and rectified immediately after Hurricane Maria to provide a dataset for emergency assessment and response to the event. Thus, although the resolution of the imagery is high (0.15 m), the geospatial rectification is imperfect. In some places, discrepancies were noticeable after overlaying our mapped landslide polygons with a 1-m lidar digital elevation model (DEM) acquired between January 2016 and March 2017 (US Geological Survey 2018). Where necessary, we edited the mapped landslide polygons to properly align with the topography. For example, some parts of the initially mapped polygons were located on the side slopes of drainages, rather than along the thalwegs of drainages. Additionally, some polygons did not properly align with fixed infrastructure (roads and houses). A similar editing process has been used for debris-flow mapping in the Oregon Coast Range (Coe et al. 2011a). When editing the landslide polygons, we retained their original shapes and sizes (i.e., lengths and widths), and the impact on the locations of headscarp points and travel distances was negligible. This, and the subsequent work by Hughes et al. (2019), indicated that maximum rectification errors and thus the maximum amount that landslide polygons were adjusted was about 3 m.

For each headscarp point, we mapped a maximum travel distance line by delineating a curvilinear centerline connecting the headscarp point to the farthest extent of visible landslide deposits (Fig. 3a). For landslide polygons containing multiple source areas, maximum travel distance lines were drawn for each headscarp point (Fig. 3b, c). The maximum travel distance lines represent the farthest distance that landslide material may have traveled. Since the travel distance lines for each of the headscarp points in a coalescing landslide share the same endpoint (Fig. 3c), the mapped travel distance for an individual source area may be overestimated. However, without detailed landslide timing and process information, we cannot differentiate the travel distances of material from individual source areas within a coalescing landslide polygon.

When a landslide travel path intersected a tributary stream (as was common for long-traveled landslides), we terminated the landslide polygon at the tributary junction if we could not definitively differentiate between landslide and flood deposits along the

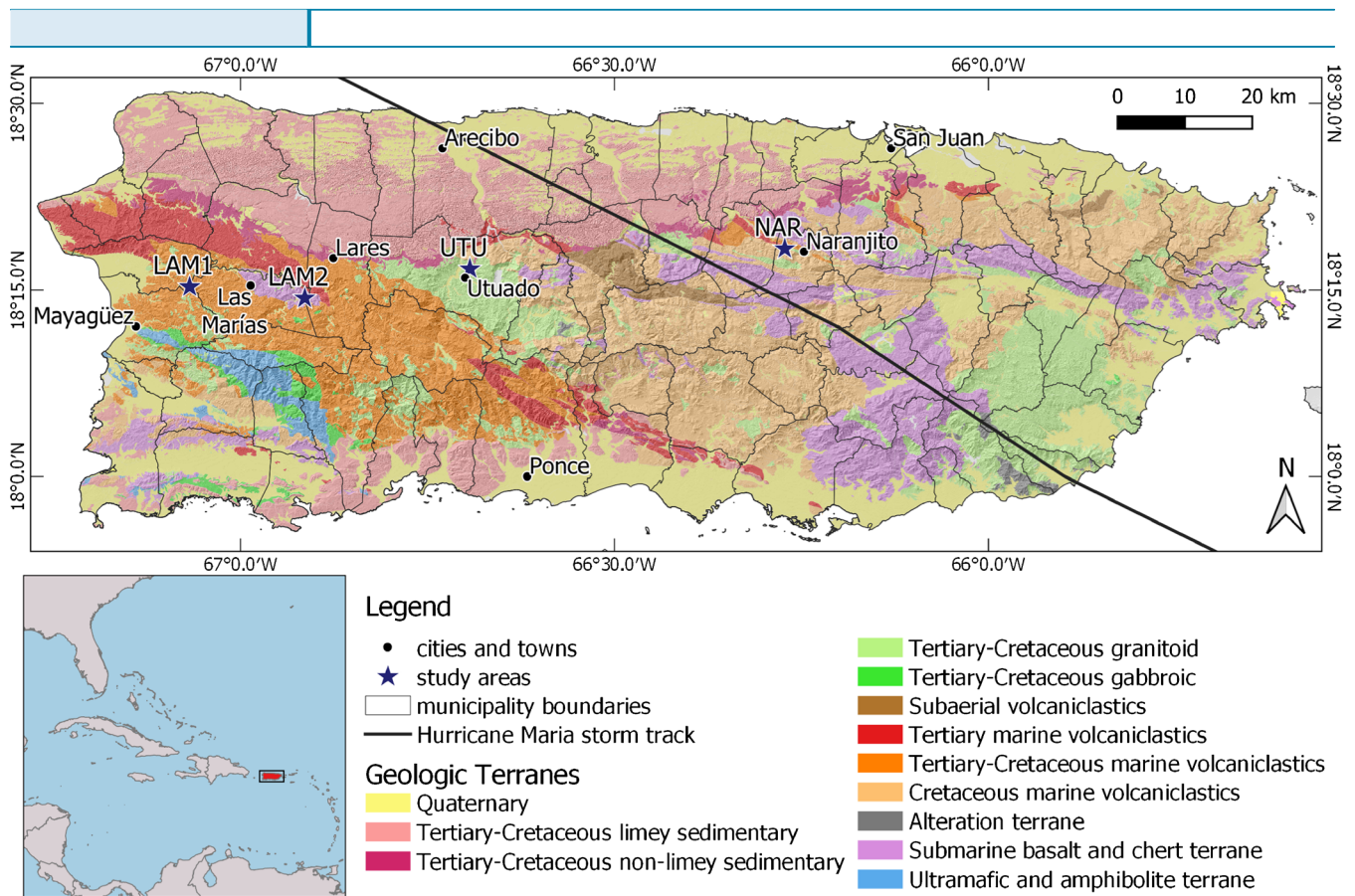


Fig. 1 Generalized geologic terranes (Bawiec 1998) on the main island of Puerto Rico and the locations of the Las Marías 1 (LAM1), Las Marías 2 (LAM2), Utuado (UTU), and Naranjito (NAR) study areas, in which landslides triggered by Hurricane Maria were mapped

adjoining stream channel (Fig. 3d). During field work, we observed that extreme flooding occurred concurrently with landsliding, causing most deposits that entered tributary streams to be fully

or partially reworked by water and were thus either not present or not readily identifiable after Hurricane Maria. To account for the presence and extent of such landslide deposits, we mapped

Table 1 Generalized geologic terranes and detailed (1:100,000) geologic units in the Las Marías 1 (LAM1), Las Marías 2 (LAM2), Utuado (UTU), and Naranjito (NAR) study areas

Study Area	Generalized Geologic Terranes ¹	Geologic Unit(s) 1:100,000 scale ²
LAM1	Marine volcaniclastics	Yauco Formation (TKy): siltstone, claystone, sandstone, limestone, and conglomerate
		Lago Garzas Formation (TKI): volcanic breccia, lava, subordinate volcanic sandstone and claystone, and interbedded calcirudite and pillowed basalt flows
		Maricao Formation (TKm): volcanic breccia, tuffaceous sandstone, mudstone, tuff, and subordinate lava and limestone
LAM2	Submarine basalt and chert	Concepcion Formation (Kco): massive basaltic lava and volcanic breccia interbedded with tuff and rare limestone lenses
UTU	Granitoid	Utuado batholith (Ku): granodiorite and subordinate quartz diorite, quartz monzonite, and diorite
NAR	Marine volcaniclastics	Los Negros Formation (Kln): basaltic breccia with some basaltic lava and subordinate sandstone and minor siltstone
		Naranjito Formation (TKn): tuff and tuffaceous epiclastic rock, volcanic sandstone, and local lava flows
		Palmarejo Formation (Tpa): volcanic sandstone interbedded with siltstone
		Hornblende quartz-diorite porphyry (TKh): porphyritic hornblende quartz diorite with minor hornblende-granodiorite, quartz monzonite, and quartz diorite

Data are from ¹ Bawiec (1998) and ² Krushensky and Schellekens (1998)

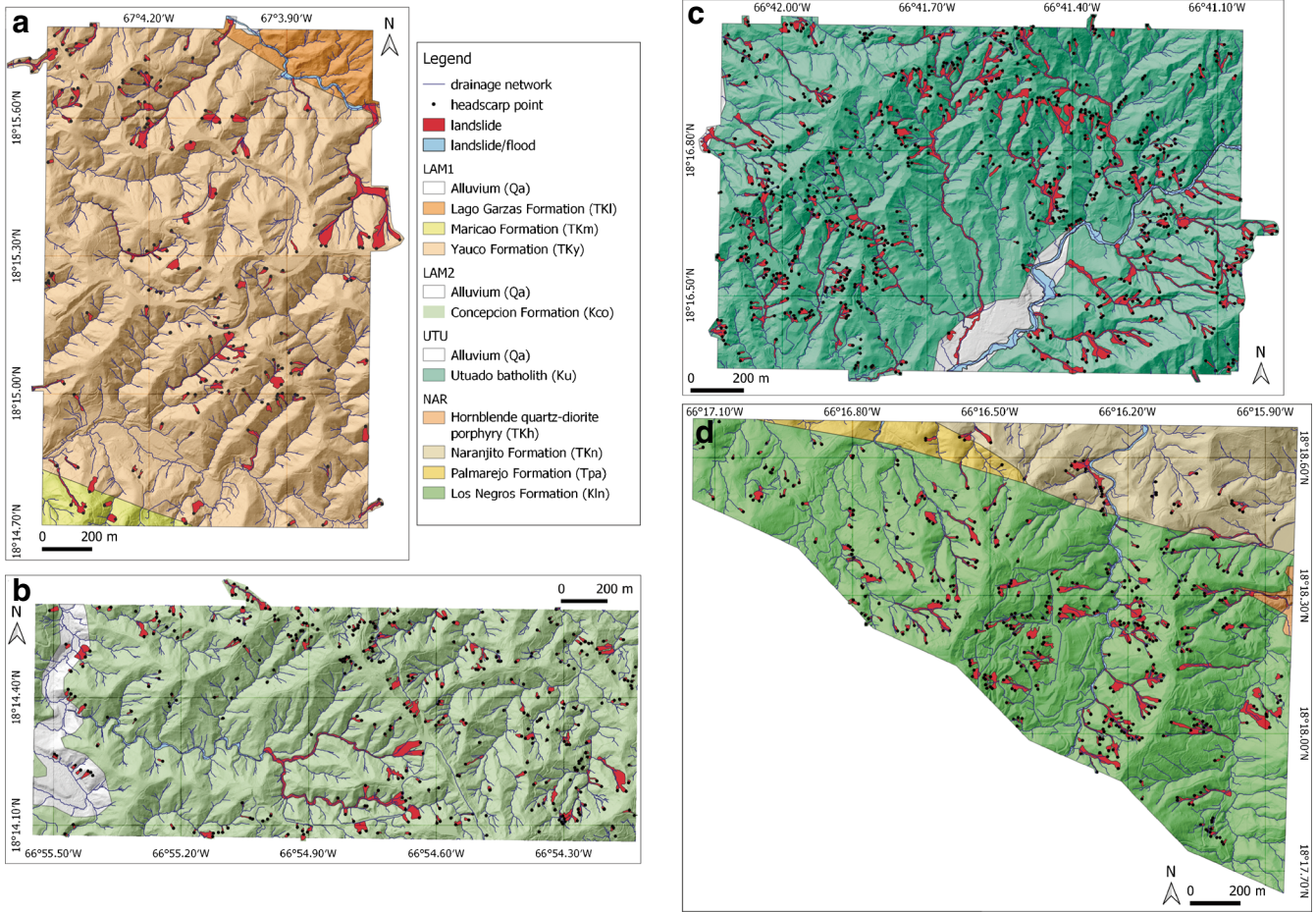


Fig. 2 Maps of the **a** LAM1, **b** LAM2, **c** UTU, and **d** NAR study areas showing mapped landslides (red), landslide/flood polygons (light blue), and headscarp points (black circles). Drainage networks are shown in dark blue and 1:100,000 scale geologic units (Table 1; Krushensky and Schellekens 1998) are overlain on a 1 m-resolution pre-event lidar hillshade (US Geological Survey 2018). As described in Table 1, the primary units in each study area are the Yauco Formation (TKy) in LAM1, the Concepcion Formation (Kco) in LAM2, the Utuado batholith (Ku) in UTU, and the Los Negros Formation (Kln) in NAR

tributary streams that intersected at least one landslide travel path and contained a combination of landslide and flood deposits; we refer to these areas as “landslide/flood polygons.” The maximum

travel distances measured for landslides intersecting a tributary stream (i.e., a landslide/flood polygon) represent minimum estimates of the travel extent because we were not able to measure the

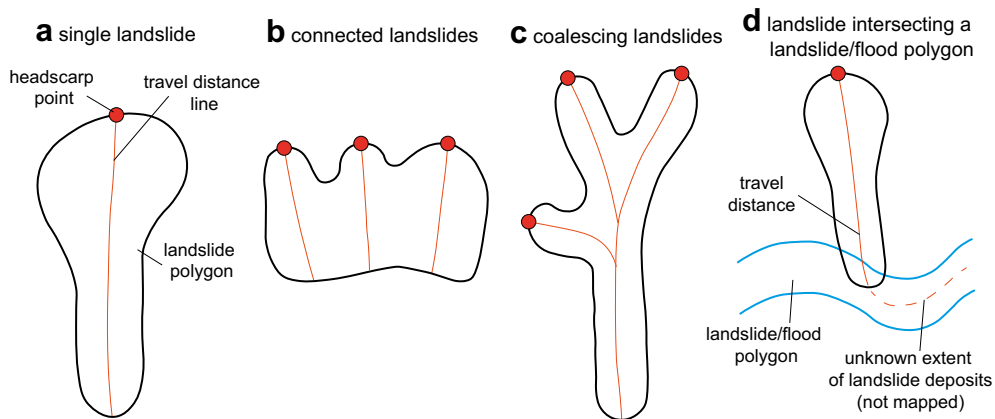


Fig. 3 Diagrams showing the methods used to map **a** single landslides, **b** connected landslides, **c** coalescing landslides, and **d** landslides intersecting landslide/flood polygons

Table 2 Number of mapped landslides and headscarp points, percent area affected by landslides, and landslide mobility characteristics for single and coalescing landslides in each study area

Study area	Bedrock geology	Landslide type	No. of mapped landslide polygons	No. of mapped headscarp points	Affected area (%)	Median area (m ²)	Median L (m)	Median H (m)	Median H/L
LAM1	Mudstone, siltstone, and sandstone (MSS)	All	100	158	3.7	303	36.0	25.5	0.73
		Single	78		1.3	254	29.7	21.7	0.74
		Multiple	22		2.4	1414	60.4	36.1	0.60
LAM2	Submarine basalt and chert (SBC)	All	298	365	3.8	104	15.2	11.8	0.76
		Single	263		1.7	89	14.3	11.1	0.77
		Multiple	35		2.1	548	35.8	26.7	0.65
NAR	Marine volcanoclastics (MVC)	All	236	398	5.7	141	20.9	12.7	0.55
		Single	174		1.6	98	16.9	9.8	0.59
		Multiple	62		4.1	839	45.6	24.3	0.45
UTU	Granodiorite (GRA)	All	401	772	8.4	89	13.9	10.1	0.67
		Single	302		1.4	62	12.1	8.8	0.71
		Multiple	99		7.1	636	46.4	20.4	0.52
All		All	1035	1693	5.4	119	17.5	11.9	0.68
		Single	817		1.5	85	14.2	10.2	0.71
		Multiple	218		3.9	715	44.3	25.2	0.52

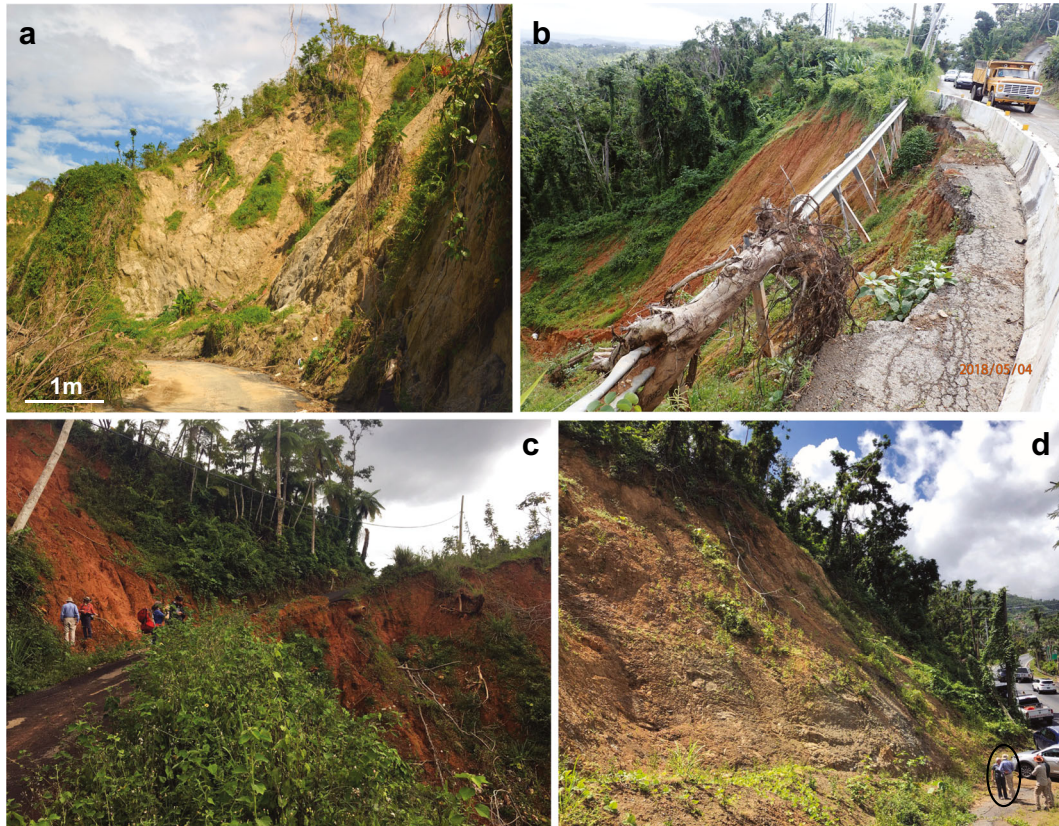


Fig. 4 Landslide source areas in soil and saprolite overlying **a** granodiorite (GRA) in Utuado (UTU; photo credit: Jason Kean); **b** mudstone, siltstone, and sandstone (MSS) in Las Marías 1 (LAM1; photo credit: Jeffrey Coe); **c** submarine basalt and chert (SBC) in Las Marías 2 (LAM2; photo credit: William Schulz); and **d** marine volcanics (MVC) in Naranjito (NAR), with people circled for scale (photo credit: Erin Bessette-Kirton)

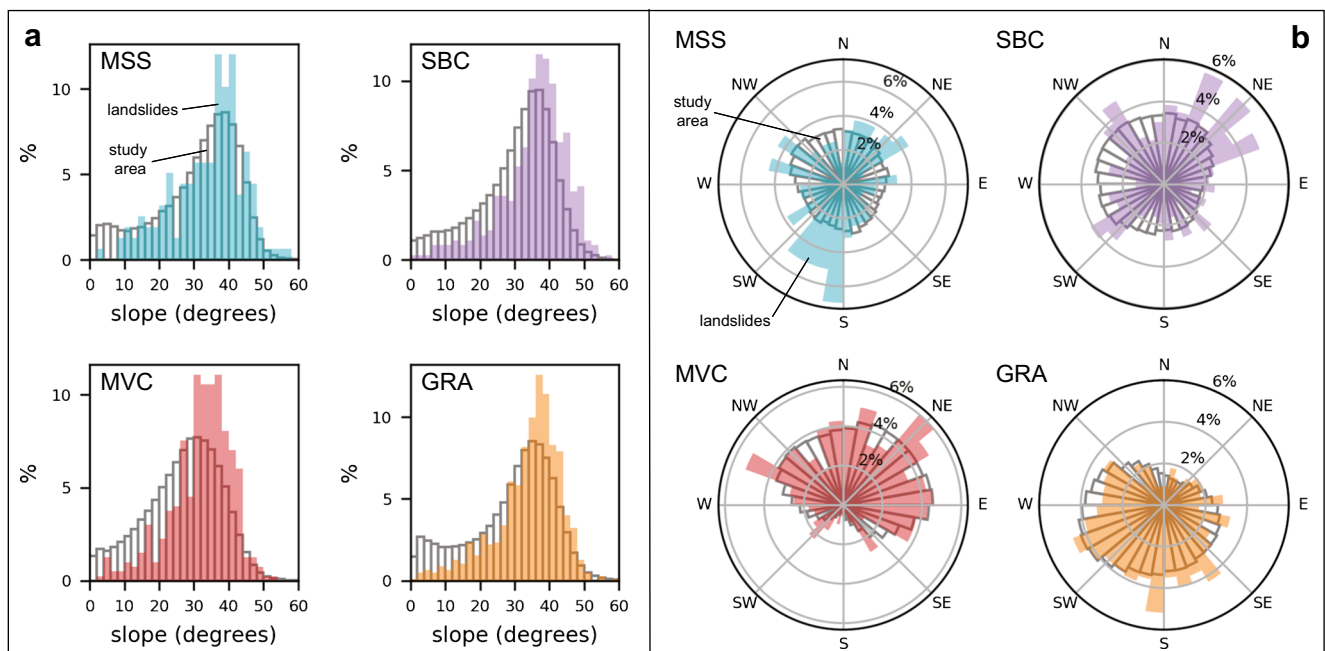


Fig. 5 Normalized slope and aspect values extracted from a 1-m resolution pre-event lidar DEM (US Geological Survey 2018), resampled to 3 m at mapped landslide headscarp locations in mudstone, siltstone, and sandstone (MSS, blue); submarine basalt and chert (SBC, purple); marine volcanics (MVC, red); and granodiorite (GRA, orange). The normalized distributions of slope and aspect in each study area are shown in gray

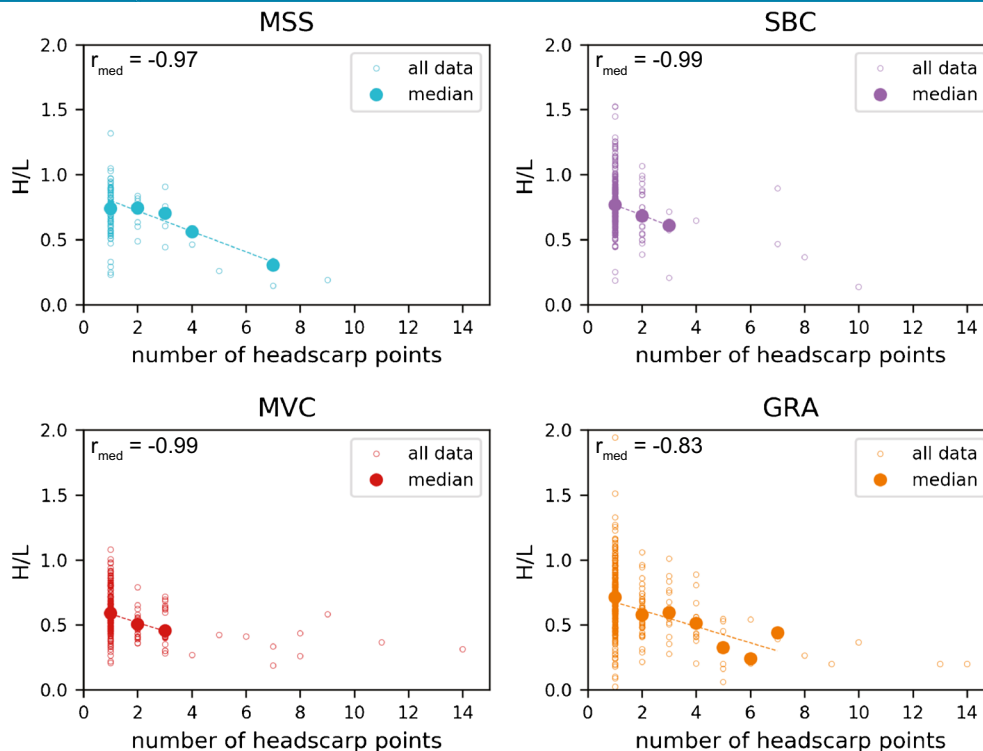


Fig. 6 Ratio of total fall height (H) to maximum travel distance (L) as a function of the number of source areas (headscarp points) per landslide for mapped landslides in mudstone, siltstone, and sandstone (MSS, blue); submarine basalt and chert (SBC, purple); marine volcanics (MVC, red); and granodiorite (GRA, orange). The median H/L was only calculated for a given number of source areas if there were three or more landslides with that number of source areas in the same formation. Landslides with more than 14 headscarp points (one in MVC and five in GRA) are not shown. Correlation coefficients (r_{med}) indicate the correlation between number of headscarp points and median H/L

distance that landslides may have traveled past the intersection of a landslide polygon and a landslide/flood polygon.

Extracting landslide characteristics by geologic formation

To assess landslide characteristics by the four major geologic formations located within our study areas (Fig. 2), we extracted source and travel attributes from our mapped landslide polygons, travel distance lines, and headscarp points. Our analysis focused on the following 1:100,000 scale bedrock geologic units (Fig. 2, Table 1): (1) Yauco Formation (TKy) in LAM1, (2) Concepcion Formation (Kco) in LAM2, (3) Utuado batholith (Ku) in UTU, and (4) Los Negros Formation (Kln) in NAR. As described in Table 1, each of these formations includes several different lithologies. For simplicity, we henceforth use the following simplifications to refer to the main geologic unit (described above) in each of our study areas: mudstone, siltstone, and sandstone (MSS) in LAM1; submarine basalt and chert (SBC) in LAM2; granodiorite (GRA) in UTU; and marine volcanics (MVC) in NAR.

We extracted the elevation, slope, and aspect at each mapped headscarp point from a 1-m resolution pre-event lidar DEM (US Geological Survey 2018), resampled to 3 m (e.g., Gillin et al. 2015). For each mapped landslide polygon, we determined the area and the number of headscarp points per polygon. Additionally, we used our mapped travel distance lines to determine (1) the difference in elevation between the headscarp point and the distal end of the deposit or fall height (H), (2) maximum travel distance (L), and (3) the ratio of H/L. To examine the influence of the drainage

network on landslide travel distance and mobility, we determined which landslides entered drainages. To do this, we intersected our mapped landslide polygons with a drainage network defined as raster cells with a contributing area greater than 200 m², where the contributing area includes only cells with concave planform curvature (D. Brien, written communication, 2019). To evaluate landslide mobility characteristics with respect to coalescence (i.e., number of contributing landslide source areas), we extracted the median values of L, H, and H/L from all of the headscarp points contained within each individual landslide polygon. All results, statistics, and analyses for landslide polygons are based on these median values.

Results

Landslide mapping

We mapped a total of 1035 landslide polygons (Fig. 2) and 1693 headscarp points (Table 2; see Bessette-Kirton et al. (2019b) for all polygon, line, and point data). The examined geologic formations contained between 100 (MSS) and 401 (GRA) landslide polygons and between 158 (MSS) and 772 (GRA) headscarp points. In GRA, 8.4% of the formation area was affected by landslides, while 3.7%, 3.8%, and 5.7% of the formation areas were affected by landslides in MSS, SBC, and MVC, respectively (Table 2). In all geologic units, single source landslides accounted for 79% of all mapped landslides but covered areas that were less than 2% of the studied formation areas. In contrast, the remaining 21% of mapped

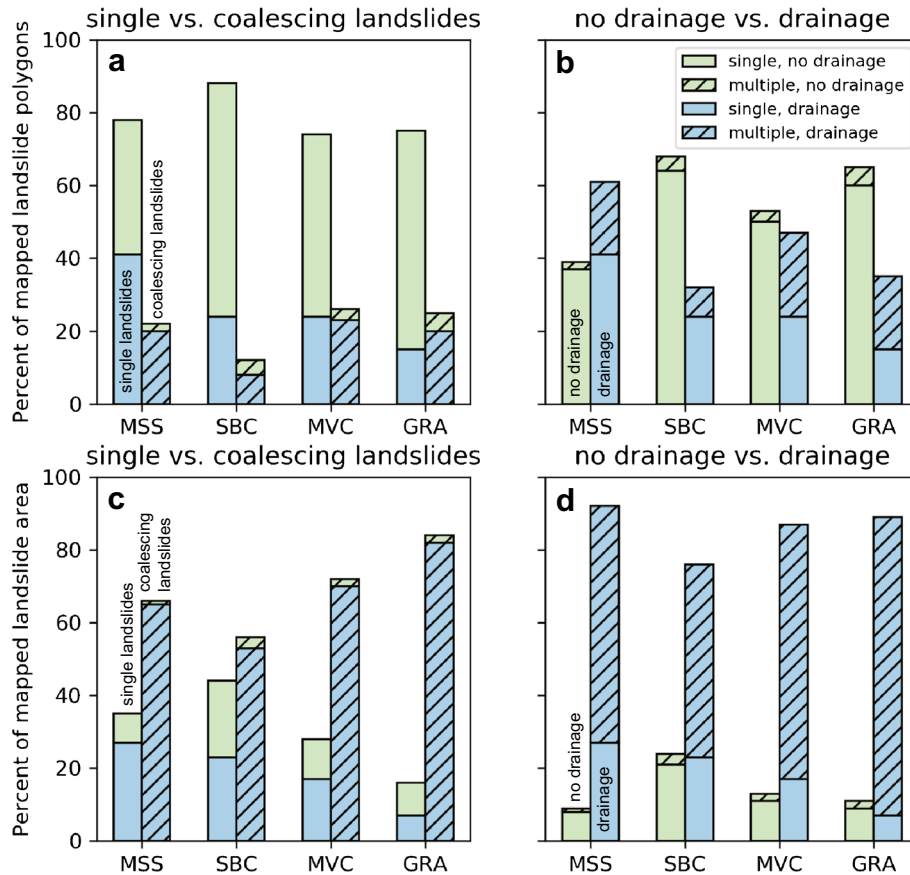


Fig. 7 a Percent of mapped landslide polygons with single and multiple source areas in each formation. b Percent of mapped landslide polygons that did or did not enter drainages in each formation. c Percent of mapped landslide area covered by landslides with single and multiple source areas in each formation. d Percent of mapped landslide area covered by landslides that did or did not enter drainages in each formation. MSS, mudstone, siltstone, and sandstone; SBC, submarine basalt and chert; MVC, marine volcanics; and GRA, granodiorite

landslides had two or more source areas and affected between 2 and 7% of the observed formation areas (Table 2).

Field observations made in the months following Hurricane Maria helped us verify our remote mapping and provided additional insight on material properties and failure types, which were generally not discernible from imagery. Based on field work, landslide material in GRA was generally sand and gravel rich with little to no cohesion, and landslides were generally < 1 m thick and < 10 m wide (Fig. 4a). Landslides in MSS, SBC, and MVC (Fig. 4b, c, and d) occurred in finer-grained silts and clays and were typically 1–2 m deep and up to several tens of meters wide. Landslides in all study areas commonly transitioned to debris flows that were much more areally extensive than the initial source areas.

Source characteristics

Across all study areas, landslides initiated from hillsides with a wide range of slope and aspect values (Fig. 5a, b). The median slope of all landslide headscarp points was 36 degrees. Since we extracted slope values at points located at the top of landslide headscarps, low slope values (< 10 degrees) may reflect flatter areas near the heads of landslides that initiated at slope crests or roads. In MSS and SBC, landslides occurred more commonly from south- to southwest-facing slopes and northeast-facing slopes, respectively, while in comparison to the uneven

distribution of slope aspects within the MVC and GRA study areas (outlined in gray), landslides initiated from no preferential aspect (Fig. 5b). Based on observations in our study areas, we did not observe any relation between slope aspect and hurricane storm track. SBC had the smallest percentage of landslides with multiple source areas (12%), while MSS, MVC, and GRA had 23%, 26%, and 25% of landslides with multiple source areas. The maximum number of source areas contained within a single landslide polygon ranged from 9 in MSS to 55 in GRA, with 18 and 10 in MVC and SBC, respectively.

Mobility characteristics

The areas of mapped landslide polygons ranged from 5 to 31,000 m² with overall median values of 85 m² for landslides with single source areas and 715 m² for landslides with multiple source areas (Table 2). The maximum travel distances (L) of mapped landslides ranged from 3 to 1128 m, with median values of 14 m and 44 m for single and coalescing landslides, respectively (Table 2). The median fall height (H) of landslides, regardless of the number of source areas, ranged from 10 m in GRA to 26 m in MSS (Table 2).

The median mobility (measured as the ratio of total fall height (H) to maximum travel distance (L)) of landslides in all geologic formations was 0.68 (Table 2). The median mobility (H/L) was

Table 3 Percent of mapped landslide polygons and percent of landslide affected area for single landslides that did not enter drainages (SND), landslides with multiple source areas that did not enter drainages (MND), single landslides that entered drainages (SD), and landslides with multiple source areas that entered drainages (MD) in each study area

Study area	Bedrock geology	SND		MND		SD		MD	
		% of mapped landslide polygons	% of landslide affected area	% of mapped landslide polygons	% of landslide affected area	% of mapped landslide polygons	% of landslide affected area	% of mapped landslide polygons	% of landslide affected area
LAM1	Mudstone, siltstone, and sandstone (MSS)	37	8	2	1	41	27	20	65
LAM2	Submarine basalt and chert (SBC)	64	21	4	3	24	23	8	53
NAR	Marine volcanics (MVC)	50	11	3	2	24	17	23	70
UTU	Granodiorite (GRA)	60	9	5	2	15	7	20	82

highest (least mobile) for landslides in SBC (0.76) and lowest (most mobile) for landslides in MVC (0.55; Table 2). In all materials, landslides with a single source area were, on average, less mobile than landslides with multiple source areas. The decrease in H/L from landslides with single to multiple source areas varied between 0.12 and 0.19. As shown in Fig. 6, the median mobility of landslides in all study areas increased linearly (median H/L decreased linearly) as the number of source areas per landslide increased.

As described above and shown in Fig. 7a, the proportions of landslides with single and multiple source areas were similar across all study areas, with a slightly smaller proportion of coalescing landslides mapped in SBC. Half or less of the single landslides in each study area entered drainage networks (between 53 in MSS and 20% in GRA), while between 69% (SBC) and 91% (MSS) of the coalescing landslides in each study area entered drainages (Fig. 7a). The proportion of landslides that entered drainages varied between study areas. In MSS, 61% of landslides entered drainages, whereas in MVC, SBC, and GRA, 47%, 32%, and 34% of landslides entered drainages, respectively (Fig. 7b). In MSS and SBC, about two-thirds of the landslides that entered drainages had a single source, whereas in MVC and GRA, the percentage of landslides that entered drainages was about equal for those with single and multiple source areas (Fig. 7b).

Although 12–26% of mapped landslide polygons had multiple source areas (Fig. 7a, b), coalescing landslides made up between 56% and 82% of the landslide affected area in each study area (Fig. 7c, d). Likewise, although fewer landslides entered drainages compared to landslides that did not enter drainages in all geologic formations except for MSS, the affected area of landslides that entered drainages was between 3 and 10 times greater than the affected area of landslides that did not enter drainages (Fig. 7d, Table 3). Although in all study areas, fewer landslides coalesced and entered drainages, those that either coalesced or entered drainages covered more area than single landslides or those that did not enter drainages. For example, in GRA, 20% of mapped landslide polygons coalesced and entered drainages, but those landslides accounted for 82% of the total landslide affected area (Table 3).

The impact that drainage networks and coalescence had on landslide mobility (H/L) is shown in Fig. 8. We examined mobility by dividing landslides into four categories: single landslides that did not enter drainages (SND), landslides with multiple source areas that did not enter drainages (MND), single landslides that entered drainages (SD), and landslides with multiple source areas that entered drainages (MD). In all geologic formations, landslides with multiple source areas that entered drainages were most mobile, and, except for MSS, single landslides that did not enter drainages were least mobile. In MSS, coalescing landslides that did not enter drainages were slightly less mobile than single landslides that did not enter drainages, which may be an artifact of sample size since there are only two landslides of this type in MSS. Figure 8 also shows that interactions with drainage networks and coalescence both independently correlated with increased landslide mobility. Comparison of SND to SD, and MND to MD, shows that both single and coalescing landslides that entered drainages had lower H/L values than landslides that did not enter drainages. Similarly, comparisons of SND to MND, and SD to MD, for all geologic formations (except for MSS), demonstrate that landslides that coalesced were more mobile than single landslides regardless of whether they entered drainages.

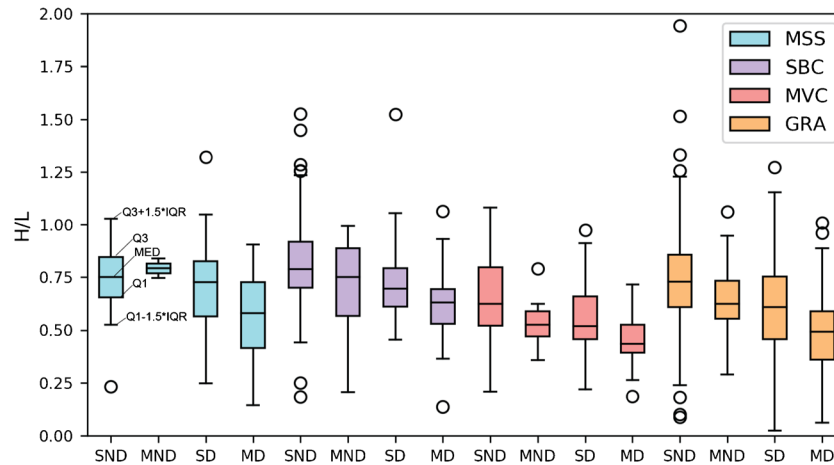


Fig. 8 Box plot distributions of the ratio of total fall height (H) to maximum travel distance (L) for single landslides that did not enter drainages (SND), landslides with multiple source areas that did not enter drainages (MND), single landslides that entered drainages (SD), and landslides with multiple source areas that entered drainages (MD) in each formation. Each plot shows the median (MED), interquartile range (IQR), and the lower and upper outlier boundaries ($Q1-1.5 \cdot IQR$ and $Q3+1.5 \cdot IQR$, respectively). Open circles indicate outliers. MSS, mudstone, siltstone, and sandstone; SBC, submarine basalt and chert; MVC, marine volcanoclastics; and GRA, granodiorite

Rainfall

To compare rainfall amounts with the mobility characteristics of landslides in each study area, we examined total storm rainfall (19–21 September 2017) distributions from Pasch et al. (2019), Ramos-Scharrón and Arima (2019), and Keellings and Hernández Ayala (2019). Pasch et al. (2019) derived rainfall from a combination of satellite data, airborne radiometry, and rain gauge data. Ramos-Scharrón and Arima (2019) interpolated rainfall data from 51 National Climatic Data Center weather stations, while Keellings and Hernández Ayala (2019) used a similar approach with data from 19 National Centers for Environmental Information stations and 28 US Geological Survey rain gauges. In our analysis, we used the ordinary kriging interpolation from Keellings and Hernández Ayala (2019) for consistency with the co-kriging methodology used by Ramos-Scharrón and Arima (2019).

Comparisons of total rainfall indicate that rainfall amounts were generally highest in the eastern and central regions of Puerto Rico and lowest on the western side of the island. However, overall differences in rainfall datasets (Fig. 9) yield inconsistencies between rainfall amounts in each study area (Table 4, Fig. 10). Data from Pasch et al. (2019) and Ramos-Scharrón and Arima (2019) indicate that MVC and GRA received more total rainfall than SBC and MSS (Table 4, Fig. 10). Conversely, data from Keellings and Hernández Ayala (2019) show that rainfall amounts in SBC and GRA were similar. While the average rainfall amounts estimated in GRA and MSS were consistent between all three datasets to within 10 and 30 mm, respectively, average rainfall amounts in MVC and SBC differed by 115 and 140 mm, respectively.

Discussion

By consistently mapping landslide travel distances, we were able to compare the mobility characteristics of over 1000 landslides that occurred during Hurricane Maria. Overall, landslides in marine volcanoclastics (MVC) were most mobile (median H/L of 0.55) followed by landslides in granodiorite (GRA; median H/L of 0.67) and mudstone, siltstone, and sandstone (MSS; median H/L of 0.73), whereas landslides that occurred in submarine basalt and

chert (SBC; median H/L of 0.76) were least mobile. While single source area landslides had a wide distribution of H/L values (< 0.1–2) with an overall median of 0.71, landslides with multiple source areas displayed smaller H/L distributions and median values as low as 0.25 (Fig. 11). Below, we assess both the intrinsic and extrinsic factors that contribute to landslide mobility as a step towards improving the understanding of variations in mobility for rainfall-induced landslides in Puerto Rico.

During Hurricane Maria, the intensity and total amount of rainfall, as well as concurrent flooding, likely enhanced landslide mobility by increasing the water content of landslides. Rainfall distribution data from Ramos-Scharrón and Arima (2019) and Keellings and Hernández Ayala (2019) showed that total rainfall was highest in MVC, which may have contributed to landslides in MVC being more mobile than in other study areas (Fig. 10). However, Pasch et al. (2019) reported the same rainfall for MVC and GRA (Table 4), yet landslides in GRA were not as mobile as those in MVC (Fig. 10). Somewhat similarly, Pasch et al. (2019) and Ramos-Scharrón and Arima (2019) report similar rainfall for MSS and SBC, whereas Keellings and Hernández Ayala (2019) reported greater rainfall in SBC than in MSS. However, landslides in MSS were more mobile than those in SBC. While rainfall is undoubtedly a contributing factor to landslide mobility, the difficulties of measuring rainfall during hurricanes resulted in variable interpretations of rainfall amounts (Fig. 9), which precludes us from drawing further conclusions about the impact of rainfall on landslide mobility. In addition to the inherent difficulty of measuring rainfall during hurricanes and the failure of rain gauges and doppler radar during Hurricane Maria, localized effects such as orographically enhanced rainfall may have produced pockets of heavy rain that were not accurately represented by any of the existing datasets.

In addition to rainfall, the effects of material characteristics, source volume, volume growth, and topographic characteristics are important considerations for landslide mobility. Initially, material properties and source area volumes affected landslide mobility. We do not have data to differentiate between source area volumes in MVC, SBC, and MSS, but field observations by Baum et al. (2018) showed that the median landslide source area

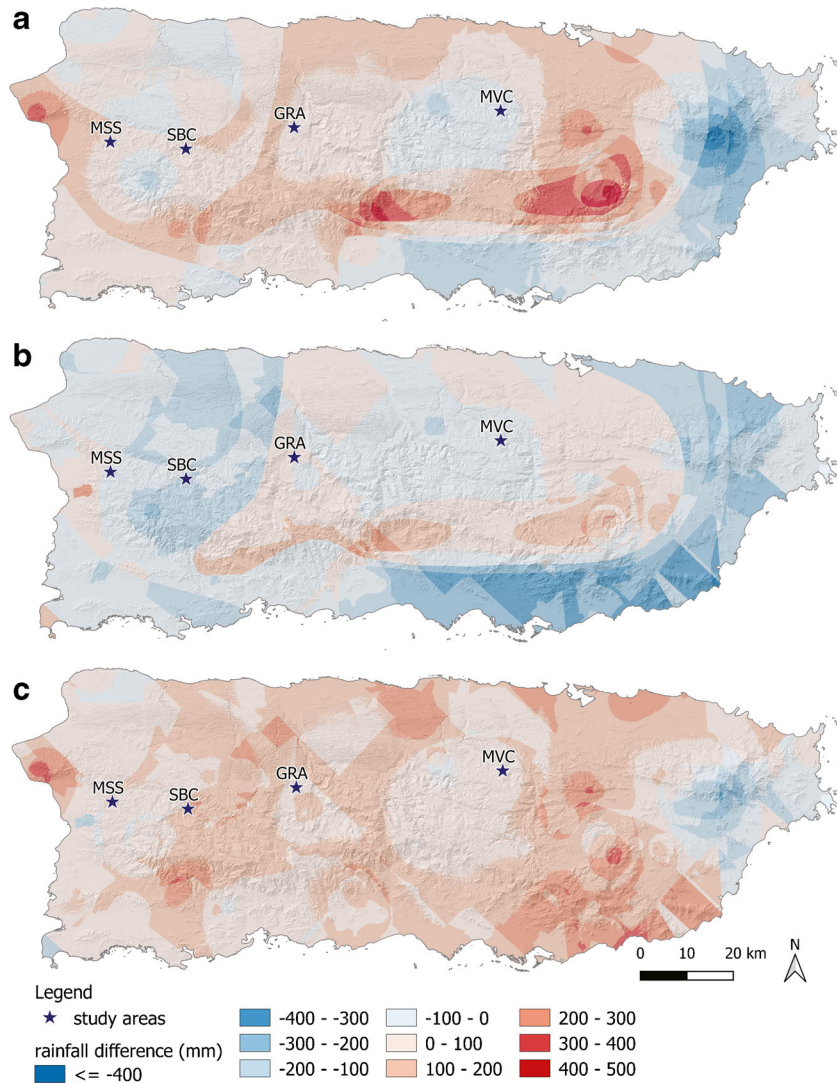


Fig. 9 Differences in rainfall distribution datasets of total storm rainfall from Hurricane Maria on the main island of Puerto Rico. Differences are between rainfall data from **a** Pasch et al. (2019) and Ramos-Scharrón and Arima (2019), **b** Pasch et al. (2019) and Keellings and Hernández Ayala (2019), and **c** Keellings and Hernández Ayala (2019) and Ramos-Scharrón and Arima (2019). MSS, mudstone, siltstone, and sandstone; SBC, submarine basalt and chert; MVC, marine volcanics; and GRA, granodiorite

volume in GRA was an order of magnitude smaller than that for landslides in the other three formations. However, landslides in GRA were generally more mobile than landslides in SBC and MSS, which is not explained by volume differences, given the well-known correlation between larger volumes and higher mobility (e.g., Corominas 1996; Legros 2002). This suggests that relatively high rainfall in GRA, material properties, or other factors also played important roles in landslide mobility. Material testing and detailed volume assessments are needed for a more thorough understanding of the intrinsic factors contributing to landslide mobility in Puerto Rico.

Our results showed that landslide mobility correlated with coalescence and drainage network interactions. The approximately linear relationships between the number of landslide source areas and median H/L yield correlation coefficients (r_{med}) between -0.83 and -0.99 (Fig. 6), indicating similar correlations with

coalescence in different geologic formations. This correlation is unsurprising when considering the large body of research showing that mobility increases as a function of landslide volume (e.g., Corominas 1996; Legros 2002) and the intuitive presumption that the number of source areas serves as a proxy for landslide volume. The increase in mobility observed for an increase in the number of source areas can be attributed to the increased volume obtained by coalescing landslides and entrainment along the landslide travel path. Material along the landslide travel path may have either been present prior to Hurricane Maria or may have been the result of landslide deposits that were emplaced earlier in the storm. Scouring along landslide travel paths from failures that occurred earlier during the hurricane could have also contributed to the increased mobility of coalescing landslides by removing barriers to landslide movement (e.g., boulders, fallen trees, or log jams). Without knowledge of entrainment rates in each study area and the timing

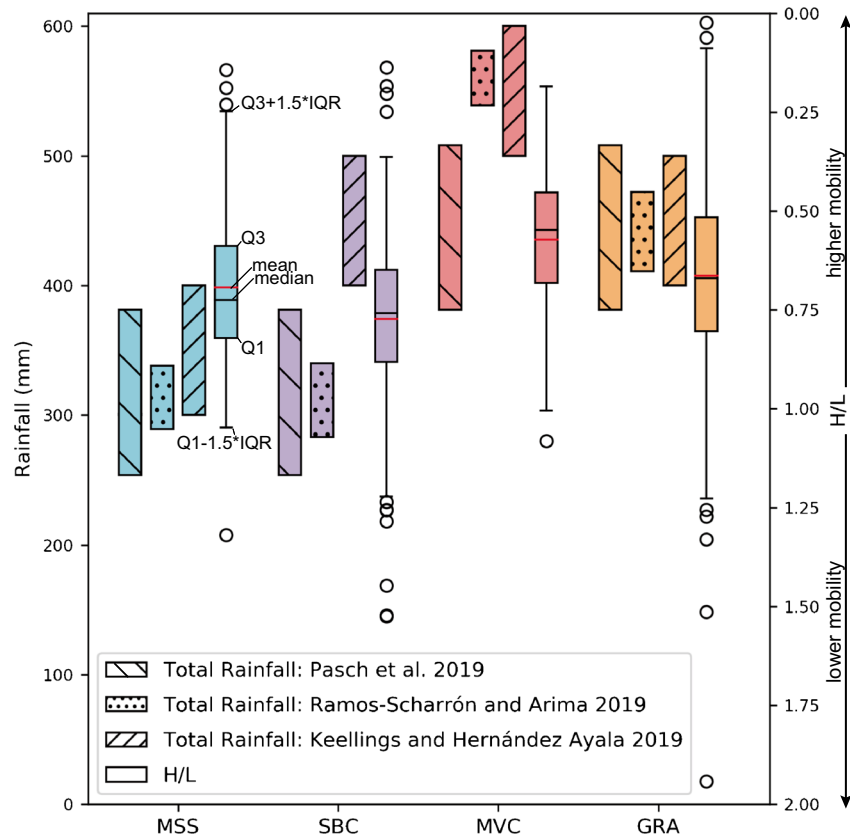


Fig. 10 Comparison of total rainfall during Hurricane Maria (Keellings and Hernández Ayala 2019; Pasch et al. 2019; Ramos-Scharrón and Arima 2019) and the distribution of landslide mobility, as measured by the ratio of total fall height (H) to maximum travel distance (L), in each study area. Each H/L distribution shows the median (black line), mean (red line), interquartile range (IQR), and the lower and upper outlier boundaries ($Q1-1.5*IQR$ and $Q3 + 1.5*IQR$, respectively). Open circles indicate outliers. MSS, mudstone, siltstone, and sandstone; SBC, submarine basalt and chert; MVC, marine volcanics; and GRA, granodiorite

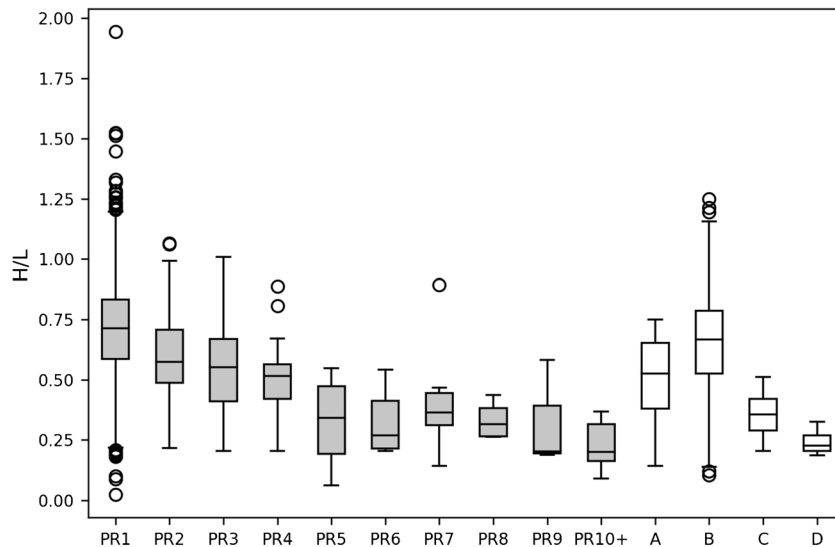


Fig. 11 Box plot distributions of the ratio of total fall height (H) to maximum travel distance (L) for mapped landslides that occurred during Hurricane Maria in Puerto Rico (PR1 through PR10+) are shown in comparison to undifferentiated debris flow and debris avalanches from around the world (A; Corominas 1996) and rainfall-triggered debris flows associated with the 2015 Gorkha Earthquake in Nepal (B; Dahlquist and West 2019), near Beijing, China (C; Li et al. 2017), and in Fukushima Prefecture, Japan (D; Okura et al. 2003). H/L distributions for landslides in Puerto Rico are shown for landslides with a single source area (PR1) through 10 or more coalescing source areas (PR10+)

Table 4 Total storm rainfall (19–21 September 2017) from Hurricane Maria in each study area, as reported from published rainfall distribution datasets

	LAM1 (MSS)	LAM2 (SBC)	NAR (MVC)	UTU (GRA)
Total rainfall from Pasch et al. (2019)	254–381 mm	254–381 mm	381–508 mm	381–508 mm
Total rainfall from Ramos-Scharrón and Arima (2019)	289–338 mm	283–340 mm	539–581 mm	411–472 mm
Total rainfall from Keellings and Hernández Ayala (2019)	300–400 mm	400–500 mm	500–600 mm	400–500 mm

of landslides that coalesced, we cannot differentiate between volume growth from contemporaneous coalescence versus entrainment and their independent effects on landslide mobility.

The increase in mobility observed for both single and coalescing landslides upon entering drainages can be explained by channelization (e.g., Guthrie et al. 2010; Coe et al. 2011b; Strom et al. 2019), entrainment of wet channel sediments (Iverson et al. 2011), and an increase in water content from mixing with floodwaters. Additionally, drainage networks provide opportunities for aggregation with other landslides. Increases in mobility because of interactions with drainage networks occur regardless of lithologic differences in initiation areas, which is consistent with our observation that drainage network interactions affected the mobility of landslides similarly in all study areas. The interconnectedness or density of drainage networks likely also impacts the degree to which landslide coalescence occurs, and further assessment of this parameter could provide additional insight into geomorphically controlled differences in mobility between study areas.

The variety in landslide sizes and types and the influence of coalescence and drainage network interactions on landslide mobility caused landslides triggered by Hurricane Maria to display a wide range of H/L values (Fig. 6). To place the mobility of landslides that occurred during Hurricane Maria in a broader context, we compared our H/L data with mobility data from landslides in other parts of the world. We compiled H/L data on undifferentiated debris flow and debris avalanches from around the world (Corominas 1996) and rainfall-triggered debris flows in the area affected by the 2015 Gorkha earthquake in Nepal (Dahlquist and West 2019), near Beijing, China (Li et al. 2017), and in Fukushima Prefecture, Japan (Okura et al. 2003). The mobility distribution of debris flows that occurred in the area affected by the Gorkha earthquake (group B in Fig. 11) was similar to the overall distribution of landslide mobility during Hurricane Maria, and with the exception of single source area landslides, coalescing debris flows during Hurricane Maria were more mobile than debris flows from Corominas (1996; group A in Fig. 11). In contrast, the debris flows in Beijing, China (group C in Fig. 11), and Fukushima Prefecture, Japan (group D in Fig. 11), have mobility distributions that are similar to debris flows in Puerto Rico with five or more source areas. Both of these events were triggered by single storm events that had similar precipitation totals to Hurricane Maria (250–535 mm over 18 h in Beijing, Li et al. 2017, and 908 mm over 5 days in Fukushima Prefecture, Okura et al. 2003), and in Beijing, landslide coalescence was also noted (Li et al. 2017). This comparison suggests that cumulative rainfall is an important controlling factor on debris-flow mobility and the occurrence of landslide coalescence across varying geographic regions and geologic materials during torrential rainstorms.

Although many of the landslides triggered by Hurricane Maria in Puerto Rico began from small source areas, landslide volumes

and mobility increased due to extreme rainfall, volume growth through coalescence and entrainment, and drainage network interactions. Other than rainfall, these factors are not required for assessing landslide initiation; however, they are critical to accurately and completely forecast landslide hazards and the risks they pose to people and infrastructure located downslope. Furthermore, increased mobility as a result of prolonged and intense precipitation events is important to consider in Puerto Rico given the frequency of landslide-triggering storms on the island (Pando et al. 2005) and because of predictions indicating the potential for increasingly frequent extreme hurricanes and tropical storms in the Atlantic Ocean basin (Knutson et al. 2010). Additional data on material strength and hydrologic properties, source area volumes, and growth rates for landslides in different geologic formations in Puerto Rico are needed to further distinguish between the influence of intrinsic material properties and extrinsic factors and to inform debris-flow hazard assessments and inundation modeling efforts in the future.

Conclusions

Our study highlights the wide range of mobility that landslides can have during torrential rainstorms in Puerto Rico and demonstrates that mobility is influenced by rainfall, geologic materials, the number of landslide source areas that coalesce, and drainage network interactions, which affect entrainment and coincidence with floodwaters. At least three quarters of mapped landslides across all geologic formations had a single source area, but those landslides accounted for far less of the total affected area and were less mobile than coalescing landslides. In the four geologic formations that we examined, landslides with multiple coalescing source areas and landslides that entered drainages were more mobile than landslides that did not. Differences in the mobility of both single and coalescing landslides between study areas indicated that landslides in submarine basalt and chert (SBC) were least mobile, while landslides in marine volcanoclastics (MVC) were most mobile. We have shown that landslide coalescence and interactions with drainage networks are important controls on mobility in Puerto Rico. Overall, extreme rainfall during Hurricane Maria increased landslide mobility, but discrepancies in rainfall datasets due to the inaccuracies associated with measuring hurricane rainfall made it difficult to draw conclusions about the effect of rainfall on landslide mobility in our select study areas. More thorough analyses of controls on mobility require improved rainfall data and additional data on material strength characteristics during flow, source volumes, and entrainment rates. Although most individual landslide source areas in Puerto Rico are generally small (<100 m²), the opportunity for landslide coalescence during large rainstorms that trigger a high density of landslides is important because of the increased potential of damaging impacts from highly mobile, long-traveled landslides.

Acknowledgments

We would like to thank Dianne Brien and six anonymous reviewers for their insightful reviews of our paper. We thank Carlos Ramos-Scharrón and Jordi Corominas for providing raw data that were used in our analyses. Any use of trade, firm, or product names is for descriptive purposes only and does not imply endorsement by the US Government.

Open Access This article is licensed under a Creative Commons Attribution 4.0 International License, which permits use, sharing, adaptation, distribution and reproduction in any medium or format, as long as you give appropriate credit to the original author(s) and the source, provide a link to the Creative Commons licence, and indicate if changes were made. The images or other third party material in this article are included in the article's Creative Commons licence, unless indicated otherwise in a credit line to the material. If material is not included in the article's Creative Commons licence and your intended use is not permitted by statutory regulation or exceeds the permitted use, you will need to obtain permission directly from the copyright holder. To view a copy of this licence, visit <http://creativecommons.org/licenses/by/4.0/>.

References

- Aaron J, McDougall S (2019) Rock avalanche mobility: the role of path material. *Eng Geol* 257:105126. <https://doi.org/10.1016/j.enggeo.2019.05.003>
- Baum RL, Cerovski-Darriau C, Schulz WH, Bessette-Kirton E, Coe JA, Smith JB, Smoczyk G (2018) Variability of hurricane Maria debris-flow source areas in Puerto Rico—implications for hazard assessment. AGU Fall Meeting, Abstract NH14A-02
- Bawiec WJ (1998) Geologic terranes of Puerto Rico. In: Bawiec WJ (ed) *Geology, geochemistry, geophysics, mineral occurrences and mineral resource assessment for the Commonwealth of Puerto Rico*, U.S. Geological Survey Open-File Report 98–38, available online only. <https://pubs.usgs.gov/of/1998/of98-038/>
- Bessette-Kirton EK, Cerovski-Darriau C, Schulz WH, Coe JA, Kean JW, Godt JW, Thomas MA, Hughes KS (2019a) Landslides triggered by hurricane Maria: assessment of an extreme event in Puerto Rico. *GSA Today* 29(6):4–10. <https://doi.org/10.1130/GSATG383A.1>
- Bessette-Kirton EK, Coe JA, Cerovski-Darriau C, Kelly MA, Schulz WH (2019b) Map data from landslides triggered by hurricane Maria in four study areas of Puerto Rico. U.S. Geological Survey data release. <https://doi.org/10.5066/P9OW4SLX>
- Bessette-Kirton EK, Coe JA, Godt JW, Kean JW, Rengers FK, Schulz WH, Baum RL, Jones ES, Staley DM (2017) Map data showing concentration of landslides caused by hurricane Maria in Puerto Rico. U.S. Geological Survey data release. <https://doi.org/10.5066/F7JD4VRF>
- Buchanan, S (2017) Federal collaboration yields radar coverage for Puerto Rico, USVI in wake of Hurricane Maria: DOD lends radars, personnel to assist NOAA with weather forecasts. <http://www.noaa.gov/media-release/federal-collaboration-yields-radar-coverage-for-puerto-rico-usvi-in-wake-of-hurricane>. Accessed April 2018
- Coe JA, Baum RL, Allstadt KE, Kochevar BF, Schmitt RG, Morgan ML, White JL, Stratton B, Hayashi TA, Kean JW (2016) Rock avalanche dynamics revealed by large-scale field mapping and seismic signals at a highly mobile avalanche in the West Salt Creek valley, western Colorado. *Geosphere* 12(2):607–631. <https://doi.org/10.1130/GES01265.1>
- Coe JA, Michael JA, Burgos MM (2011a) Map of debris flows caused by rainfall during 1996 in parts of the Reedsport and Deer Head Point quadrangles, Douglas County, southern Coast Range, Oregon. U.S. Geological Survey Open-File Report 2011–1150, 9 p. pamphlet, 1 sheet, scale 1:12,000. <https://pubs.usgs.gov/of/2011/1150/>
- Coe JA, Reid ME, Brien DL, Michael JA (2011b) Assessment of topographic and drainage network controls on debris-flow travel distance along the west coast of the United States. In: *Proceedings of the 5th International Conference on Debris Flow Hazards and Mitigation*, Padua, Italy, June, 2011, *Italian Journal of Engineering Geology and Environment*, pp 199–209. <https://doi.org/10.4408/IJEGE.2011-03.B-024>
- Collins BD, Reid ME (2019) Enhanced landslide mobility by basal liquefaction: the 2014 state route 530 (Oso). *Washington landslide Geol Soc Am Bull* 132:451–476. <https://doi.org/10.1130/B35146.1>
- Collison AJC, Anderson MG (1996) Using a combined slope hydrology/stability model to identify suitable conditions for landslide prevention by vegetation in the humid tropics. *Earth Surf Proc Land* 21:737–747. [https://doi.org/10.1002/\(SICI\)1096-9837\(199608\)21:8<737::AID-ESP674>3.0.CO;2-F](https://doi.org/10.1002/(SICI)1096-9837(199608)21:8<737::AID-ESP674>3.0.CO;2-F)
- Corominas J (1996) The angle of reach as a mobility index for small and large landslides. *Can Geotech J* 33:260–271
- Dahlquist MP, West AJ (2019) Initiation and runout of post-seismic debris flows: insights from the 2015 Gorkha earthquake. *Geophys Res Lett* 46(16):9658–9668. <https://doi.org/10.1029/2019gl083548>
- Dai FC, Lee CF (2002) Landslide characteristics and slope instability modeling using GIS, Lantau Island, Hong Kong. *Geomorphology* 42:213–228
- Davies TR, McSaveney MJ, Hodgson KA (1999) A fragmentation-spreading model for long-runout rock avalanches. *Can Geotech J* 36(6):1096–1110. <https://doi.org/10.1139/t99-067>
- Devoli G, De Blasio FV, Elverhøi A, Høeg K (2009) Statistical analysis of landslide events in Central America and their run-out distance. *Geotech Geol Eng* 27:23–42. <https://doi.org/10.1007/s10706-008-9209-0>
- Ellen SD, Mark RK, Cannon SH, Knifong DL (1993) Map of debris-flow hazard in the Honolulu District of Oahu, Hawaii. U.S. Geological Survey Open-File Report 93–213. <https://pubs.usgs.gov/of/1993/of93-213/>
- Evans SG, Guthrie RH, Roberts NJ, Bishop NF (2007) The disastrous 17 February 2006 rockslide debris avalanche on Leyte Island, Philippines: a catastrophic landslide in tropical mountain terrain. *Nat Hazard Earth Sys* 7(1):89–101
- Gillin CP, Bailey SW, McGuire KJ, Prisley SP (2015) Evaluation of lidar-derived DEMs through terrain analysis and field comparison. *Photogramm Eng Remote Sensing* 81(5):387–396. <https://doi.org/10.14358/PERS.81.5.387>
- Guariguata MR, Larsen MC (1990) Preliminary map showing landslides in El Yunque quadrangle, Puerto Rico. U.S. Geological Survey Open-File Report 89–257, scale 1:20,000, 1 sheet
- Guthrie RH, Hockin A, Colquhoun L, Nagy T, Evans SG, Ayles C (2010) An examination of controls on debris flow mobility: evidence from coastal British Columbia. *Geomorphology* 114(4):601–613. <https://doi.org/10.1016/j.geomorph.2009.09.021>
- Harp EL, Reid ME, Michael JA (2004) Hazard analysis of landslides triggered by Typhoon Chatáan on July 2, 2002, in Chuuk State, Federated States of Micronesia. U.S. Geological Survey Open-File Report 2004–1348
- Heim A (1932) *Landslides and human lives (Bergsturz und Menschenleben)*. Bi-Tech Publishers, Vancouver, BC
- Hennessy-Fiske, M (2017) In one Puerto Rico mountain town, a wall of mud came crashing down. <http://www.latimes.com/nation/la-na-puerto-rico-landslide-20170924-story.html>. Accessed April 2018
- Hughes KS, Bayouth García D, Martínez Milián GO, Schulz WH, and Baum RL (2019) Map of slope-failure locations in Puerto Rico after hurricane Maria. U.S. Geological Survey data release. <https://doi.org/10.5066/P9BVM7D4>
- Hungr O, Evans SG (2004) Entrainment of debris in rock avalanches: an analysis of a long run-out mechanism. *Geol Soc Am Bull* 116(910):12401252. <https://doi.org/10.1130/B25362.1>
- Hungr O, Leroueil S, Picarelli L (2014) The Varnes classification of landslide types, an update. *Landslides* 11(2):167–194. <https://doi.org/10.1007/s10346-013-0436-y>
- Irizarry Álvarez, F (2017) Mueren tres hermanas por derrumbe en Utuado tras paso de María. <http://www.primerahora.com/noticias/puerto-rico/nota/muerentres-hermanaspor derrumbeenutuadotraspasodemaria-1246727/>. Accessed July 2018
- Iverson RM (1997) The physics of debris flows. *Rev Geophys* 35(3):245–296
- Iverson RM, George DL, Allstadt K, Reid MR, Collins BD, Vallance JW, Schilling SP, Godt JW, Cannon CM, Magirl CS, Baum RL, Coe JA, Schulz WH, and Bower JB (2015) Landslide mobility and hazards: implications of the 2014 Oso disaster. *Earth Planet Sc Lett* 412:197–208. <https://doi.org/10.1016/j.epsl.2014.12.020>
- Iverson RM, Reid ME, Logan M, LaHusen RG, Godt JW, Griswold JP (2011) Positive feedback and momentum growth during debris-flow entrainment of wet bed sediment. *Nat Geosci* 4:116–121. <https://doi.org/10.1038/NGEO1040>
- Jibson RW (1989) Debris flows in southern Puerto Rico. In: Schultz AP, Jibson RW (eds) *Landslide processes of the eastern United States and Puerto Rico*, Geological Society of America special paper 236, pp 29–56. <https://doi.org/10.1130/SPE236-p29>
- Jibson RW (1992) The Mamayas, Puerto Rico, landslide disaster of October 7, 1985. In: Slosson JE, Keene AG, Johnson JA (eds) *Landslides/landslide mitigation Geological Society of America reviews in engineering geology IX*. Boulder, Colorado, pp 37–54
- Kean JW, Staley DM, Lancaster J, Rengers FK, Swanson B, Coe JA, Hernandez J, Sigman A, Allstadt KE, Lindsay D (2019) Inundation, flow dynamics, and damage in the 9

- January 2018 Montecito debris flow event, California, USA: Opportunities and challenges for post-wildfire risk assessment. *Geosphere*. <https://doi.org/10.1130/GES02048.1>, 15, 1140, 1163
- Keellings D, Hernández Ayala JJ (2019) Extreme rainfall associated with hurricane Maria over Puerto Rico and its connections to climate variability and change. *Geophys Res Lett* 46(5):2964–2973. <https://doi.org/10.1029/2019GL082077>
- Knutson TR, McBride JL, Chan J, Emanuel K, Holland G, Landsea C, Held I, Kossin JP, Srivastava AK, Sugi M (2010) Tropical cyclones and climate change. *Nat Geosci* 3:157–163. <https://doi.org/10.1038/ngeo779>
- Krushensky RD, Schellekens JH (1998) Geology of Puerto Rico. In: Bawiec WJ (ed.) *Geology, geochemistry, geophysics, mineral occurrences and mineral resource assessment for the Commonwealth of Puerto Rico*, U.S. Geological Survey Open-File Report 98–38, available online only, <https://pubs.usgs.gov/of/1998/of98-038/>
- Larsen MC, Parks JE (1998) Map showing landslide susceptibility in the Comerío Municipality, Puerto Rico. U.S. Geological Survey Open-File Report 98–566
- Larsen MC, Santiago M, Jibson R, Questell E (2004) Map showing susceptibility to rainfall-triggered landslides in the municipality of Ponce, Puerto Rico. U.S. Geological Survey Scientific Investigations Map I-2818, scale 1:30,000, 1 sheet
- Larsen MC, Torres-Sánchez AJ (1992) Landslides triggered by hurricane Hugo in eastern Puerto Rico, September 1989. *Caribb J Sci* 28(3–4):113–125
- Larsen MC, Torres-Sánchez AJ (1998) The frequency and distribution of recent landslides in three montane tropical regions of Puerto Rico. *Geomorphology* 24(4):309–331. [https://doi.org/10.1016/S0169-555X\(98\)00023-3](https://doi.org/10.1016/S0169-555X(98)00023-3)
- Legros F (2002) The mobility of long-runout landslides. *Eng Geol* 63:301–331
- Lepore C, Kamal SA, Shanahan P, Bras RL (2012) Rainfall-induced landslide susceptibility zonation of Puerto Rico. *Environ Earth Sci* 66(6):1667–1681. <https://doi.org/10.1007/s12665-011-0976-1>
- Li Y, Ma C, Wang Y (2017) Landslides and debris flows caused by an extreme rainstorm on 21 July 2012 in mountains near Beijing, China. *Bull Eng Geol Environ* 78(2):1265–1280. <https://doi.org/10.1007/s10064-017-1187-0>
- Liao Z, Hong Y, Wang J, Fukuoka H, Sassa K, Karnawati D, Fathani F (2010) Prototyping an experimental early warning system for rainfall-induced landslides in Indonesia using satellite remote sensing and geospatial datasets. *Landslides* 7(3):317–324. <https://doi.org/10.1007/s10346-010-0219-7>
- Manzanal D, Dremptic V, Haddad B, Pastor M, Martin Stickle M, Mira P (2016) Application of a new rheological model to rock avalanches: an SPH approach. *Rock Mech Rock Eng* 49(6):2353–2372. <https://doi.org/10.1007/s00603-015-0909-5>
- Monroe WH (1979) Map showing landslides and areas of susceptibility to landsliding in Puerto Rico. U.S. Geological Survey Miscellaneous Investigations Series Map I-1148, scale 1:240,000, 1 sheet National Weather Service (2017) Public information statement. <https://www.weather.gov/media/serfc/PNSQPESJU2.pdf>. Accessed April 2018
- Okura Y, Kitahara H, Kawanami A, Kurokawa U (2003) Topography and volume effects on travel distance of surface failure. *Eng Geol* 67(3–4):243–254. [https://doi.org/10.1016/S0013-7952\(02\)00183-7](https://doi.org/10.1016/S0013-7952(02)00183-7)
- Pando MA, Ruiz ME, and Larsen MC (2005) Rainfall-induced landslides in Puerto Rico: an overview. In: *Proceedings GeoFrontiers congress 2005*, Austin, Texas, pp 2911–2925. [https://doi.org/10.1061/=40787\(166\)25](https://doi.org/10.1061/=40787(166)25)
- Pasch RJ, Penny AB, Berg R (2019) National hurricane center tropical cyclone report, Hurricane Maria (AL152017), 16–30 September 2017. https://www.nhc.noaa.gov/data/tcr/AL152017_Maria.pdf
- Quantum Spatial, Inc. (2017) FEMA PR imagery. <https://s3.amazonaws.com/fema-cap-imagery/Others/Maria>. Accessed October 2017
- Ramos-Scharrón CE, Arima E (2019) Hurricane María's precipitation signature in Puerto Rico: a conceivable presage of rains to come. *Sci Rep* 9(1):1–7. <https://doi.org/10.1038/s41598-019-52198-2>
- Reid ME, Coe JA, Brien DL (2016) Forecasting inundation from debris flows that grow volumetrically during travel, with application to the Oregon coast range, USA. *Geomorphology* 273:396–411. <https://doi.org/10.1016/j.geomorph.2016.07.039>
- Santi PM, Mathewson CC (1988) What happens between the scar and the fan? The behavior of a debris flow in motion. In: Fragaszy RJ (ed) *24th annual symposium on engineering geology and soils engineering*. Washington State University, Washington, DC, pp 73–78
- Sassa K (1985) The mechanism of debris flow. In: *Proceedings of XI International Conference on Soil Mechanics and Foundation Engineering*, San Francisco. A.A. Balkema, Rotterdam, the Netherlands, pp 1173–1176
- Sassa K, Wang G (2005) Mechanism of landslide-triggered debris flows: liquefaction phenomena due to the undrained loading of torrent deposits. In: Jakob M, Hungr O (eds) *Debris-flow hazards and related phenomena*. Springer, Berlin, Heidelberg, pp 81–104
- Schneider D, Huggel C, Haeblerli W, Kaitna R (2011) Unraveling driving factors for large rock-ice avalanche mobility. *Earth Surf Proc Land* 36(14):1948–1966. <https://doi.org/10.1002/esp.2218>
- Strom A, Li L, Lan H (2019) Rock avalanche mobility: optimal characterization and effects of confinement. *Landslides*. 16:1437–1452. <https://doi.org/10.1007/s10346-019-01181-z>
- Terzaghi K (1950) Mechanism of landslides. In: Paige S (ed) *Application of geology to engineering practice (Berkey volume)*. Geological Society of America, New York, pp 83–124
- U.S. Geological Survey (2017) Hurricane Maria's water footprint. <https://owi.usgs.gov/vizlab/hurricane-maria>. Accessed December 2019
- U.S. Geological Survey (2018) USGS NED original product resolution PR Puerto Rico 2015. <http://nationalmap.gov/elevation.html>. Accessed October 2018
- Vieira BC, Fernandes NF, Filho OA (2010) Shallow landslide prediction in the Sierra do Mar, Sao Paulo, Brazil. *Nat Hazard Earth Sys* 10:1829–1837. <https://doi.org/10.5194/nhess-10-1829-2010>

E. K. Bessette-Kirton · J. A. Coe · W. H. Schulz · M. M. Einbund

US Geological Survey,
Geologic Hazards Science Center,
Golden, CO, USA

E. K. Bessette-Kirton (✉)

Department of Geology and Geophysics,
University of Utah,
Salt Lake City, UT, USA
Email: erin.bessette.kirton@utah.edu

C. Cerovski-Darriau

US Geological Survey,
Geology, Minerals, Energy, and Geophysics Science Center,
Moffett Field, CA, USA